



## Improving global paleogeography since the late Paleozoic using paleobiology

Wenchao Cao<sup>\*1</sup>, Sabin Zahirovic<sup>1</sup>, Nicolas Flament<sup>†1</sup>, Simon Williams<sup>1</sup>, Jan Golonka<sup>2</sup> and R. Dietmar Müller<sup>1</sup>

5 <sup>1</sup> EarthByte Group, School of Geosciences, The University of Sydney, NSW 2006, Australia

<sup>2</sup> Faculty of Geology, Geophysics and Environmental Protection, AGH University of Science and Technology, Mickiewicza 30, 30-059 Kraków, Poland

*\*Correspondence to:* Wenchao Cao (wenchao.cao@sydney.edu.au)

10 <sup>†</sup>Current address: School of Earth and Environmental Sciences, University of Wollongong, Northfields Avenue, Wollongong, New South Wales 2522, Australia

**Abstract.** Paleogeographic reconstructions are important to understand Earth's tectonic evolution, past eustatic and regional sea level change, hydrocarbon genesis, and to constrain and interpret the dynamic topography predicted by time-dependent global mantle convection models. Several global paleogeographic maps have been compiled and published but they are generally presented as static maps with varying temporal resolution and fixed spatial resolution. Existing global paleogeographic maps are also tied to a particular plate motion model, making it difficult to link them to alternative digital plate tectonic reconstructions. To address this limitation, we developed a workflow to reverse-engineer global paleogeographic maps to their present-day coordinates and enable them to be linked to any tectonic reconstruction. Published paleogeographic compilations are also tied to fixed input datasets. We used fossil data from the Paleobiology Database to identify inconsistencies between fossils paleo-environments and published paleogeographic maps, and to improve the location of inferred terrestrial-marine boundaries by resolving these inconsistencies. As a result, the overall consistency ratio between the paleogeography and fossil collections was improved from 76.9% to 96.1%. We estimated the surface areas of global paleogeographic features (shallow marine environments, landmasses, mountains and ice sheets), and reconstructed the global continental flooding history since the late Paleozoic based on the amended paleogeographies. Finally, we discuss the relationships between emerged land area and total continental crust area through time, continental growth models, and strontium isotope (<sup>87</sup>Sr/<sup>86</sup>Sr) signatures in ocean water. Our study highlights the flexibility of digital paleogeographic models linked to state-of-the-art plate tectonic reconstructions in order to better understand the interplay of continental growth and eustasy, with wider implications for understanding Earth's paleotopography, ocean circulation, and the role of mantle convection in shaping long-wavelength topography.

### 1 Introduction

Paleogeography is widely used in a range of fields including paleoclimatology, plate tectonic



40 reconstructions, paleobiogeography, resource exploration and geodynamics. Several global deep-time  
paleogeographic compilations have been published (e.g. Blakey, 2008; Golonka et al., 2006; Ronov, et  
al., 1984, 1989; Scotese, 2004; Smith et al., 1994). However, they are generally presented as static  
45 paleogeographic snapshots with varying temporal resolution and fixed spatial resolution, and are tied to  
a particular plate motion model. This makes it difficult to link them to alternative digital plate tectonic  
reconstructions, and to update paleogeographic maps when plate motion models are improved. It is  
therefore challenging to use paleogeographic maps to help constrain or interpret numerical models of  
mantle convection that predict long-wavelength topography (Gurnis et al., 1998; Spasojevic and Gurnis,  
2012) based on different tectonic reconstructions, or as an input to models of past ocean and  
atmosphere circulation/climate (Goddéris et al., 2014; Golonka et al., 1994) and models of past  
50 erosion/sedimentation (Salles et al., 2017).

In order to address this issue, we developed a workflow to reverse-engineer published  
paleogeographies to their corresponding present-day coordinates so that the geometries could be  
attached to any plate motion model. This was the first step towards the construction of paleogeographic  
55 maps with flexible spatial and temporal resolutions that are more easily testable and expandable with  
the incorporation of new paleo-environmental datasets (e.g. Wright et al., 2013). In this study, we used  
a set of global paleogeographic maps (Golonka et al., 2006) covering the entire Phanerozoic time  
period as the base paleogeographic model. We reverse-engineered these global paleogeographic maps  
to their present-day coordinates and then reconstructed them using the plate motion model of Matthews  
60 et al. (2016). Subsequently, we used fossil data from the Paleobiology Database (<https://paleobiodb.org>)  
to identify inconsistencies between fossils paleo-environments and the paleogeographic maps, and to  
improve the location of inferred terrestrial-marine boundaries by resolving these inconsistencies.  
Finally, we used the improved reconstructed paleogeographies to estimate the surface areas of global  
paleogeographic features (shallow marine environments, landmasses, mountains and ice sheets), to  
65 investigate the global continental flooding history since the Devonian and compare it with global sea  
level change over time (Haq et al., 1987; Haq et al., 2008; Müller et al., 2008). In addition, we  
discussed the evolution of the modelled emerged land area and total continental area in connection with  
continental growth models, the strontium isotope ( $^{87}\text{Sr}/^{86}\text{Sr}$ ) signature from the proxy records (Flament  
et al., 2013; van der Meer et al., 2017), and the assembly and breakup of Pangea.

70

## 2 Data and Paleogeographic Model

The data used in this study are global paleogeographic maps and paleontological data for the last 402  
Myr, which originate from the set of paleo-maps produced by Golonka et al. (2006) and the  
75 Paleobiology Database (<https://paleobiodb.org>), respectively. The global paleogeographic compilation  
by Golonka et al. (2006), spanning the entire Phanerozoic, is divided into 32 time-interval maps using  
the time scale of Sloss (1988) (Table 1). Each map is a compilation of paleolithofacies and paleo-  
environments for each geological time interval. These paleogeographic reconstructions illustrate the



80 changing configuration of ice sheets, mountains, landmasses, shallow marine environments (inclusive  
of shallow seas and continental slopes) and deep oceans during the last 544 million years.

85 The paleogeographic maps of Golonka et al. (2006) were constructed using a plate tectonic model  
available in the Supplement of Golonka (2007), which described the relative motions between plates  
and terranes. In this rotation model, paleomagnetic data were used to constrain the paleolatitudinal  
positions of continents and rotation of plates, and hot spots, where applicable, were used as reference  
points to calculate paleolongitudes (Golonka, 2007). This rotation model is necessary to accurately  
reverse-engineer these paleogeographies (Golonka et al., 2006) to their present-day coordinates so that  
90 they can be attached to any modern plate motion model. The relative plate motions of Golonka (2006,  
2007) are similar to those in Scotese (2004).

95 Here, we use a global plate kinematic model to reconstruct paleogeographies back in time from  
present-day locations. The global tectonic reconstruction of Matthews et al. (2016), with continuously  
closing plate boundaries from 410-0 Ma, is primarily constructed from a Mesozoic and Cenozoic plate  
model (230-0 Ma) (Müller et al., 2016) and a Paleozoic model (410-250 Ma) (Domeier and Torsvik,  
2014). This model is a relative plate motion model that is ultimately tied to Earth's spin axis through an  
absolute reference frame (Matthews et al., 2016).

100

The Paleobiology Database (<https://paleobiodb.org>) is a compilation of global fossil data covering deep  
geological time. All fossils in the database are associated with detailed metadata, including the time  
range (typically biostratigraphic age), present-day geographic coordinates, host lithology, and paleo-  
105 environment. Figure 1 visualizes global fossil distribution and shows the total numbers of fossil  
collections on Earth since the Devonian period. The documented fossils are unevenly distributed both  
spatially and temporally, largely due to the differences in fossil preservation and the spatial sampling  
biases of fossil localities. For this study, a total of 57,854 fossil collections with temporal and paleo-  
environmental assignments from 402 to 2 Ma were downloaded from the database on 7 September  
110 2016.

### 3 Method

115

The methodology mainly involves the processes of paleogeographic reverse-engineering, subsequent  
reconstructing in another rotation model and eventually improving using paleobiology data. Figure 2  
illustrates a generalized workflow that can be applied to any paleogeography model. In order to



represent the paleogeographic maps as digital geographic geometries, they are first georeferenced using  
120 the original projection and coordinate system (such as global Mollweide in Golonka et al., 2006), and  
then reprojected into the WGS84 geographic coordinate system. The resulting maps are then attached  
to the original rotation model using the open-source and cross-platform plate reconstruction software,  
GPlates ([www.gplates.org](http://www.gplates.org)). Every plate is then assigned a unique plate ID that defines the rotation  
rules in geological times so that the paleogeographies can be rotated back to their present-day  
125 coordinates (see example in Figs. 3a, b). We use present-day coastlines and terrane boundaries with the  
plate IDs of Golonka (2007) as a reference to refine rotations and ensure a high accuracy of the reverse  
engineering.

When the paleogeographic maps in present-day coordinates are attached to a new reconstruction model,  
130 e.g. Matthews et al. (2016) as used in this study, the resulting paleogeographies contain gaps (Fig. 3c,  
pink) and overlaps between neighboring polygons, when compared to the original reconstruction (Fig.  
3a). These gaps and overlaps essentially arise from the differences in the reconstructions described in  
Matthews et al. (2016) and Golonka et al. (2006). The reconstruction of Golonka et al. (2006) typically  
has a tighter fit of the major continents within Pangea prior to the supercontinent breakup. In addition,  
135 this reconstruction contains a different plate motion history and block boundaries definitions in regions  
of complex continental deformation, for example along active continental margins (e.g. Himalayas,  
western North America, Fig. 3c).

The gaps and overlaps cause changes in the total areas of paleogeographies at different time intervals,  
140 becoming larger or smaller, when compared with the original paleo-maps (Golonka et al., 2006). The  
gaps can be fixed by interactively extending the outlines of the polygons in a GIS platform to make the  
plates connect as in the original paleo-maps (Fig. 3a, c and d). The resulting paleogeographies with  
fixed gaps (Fig. 3d) change to different extent in total area compared with the original  
paleogeographies (Golonka et al., 2006). The total areal variations range from the maximum 5.8% to  
145 the minimum -2.7%, with an average of -1.4%. To avoid artefacts introduced from overlapping  
paleogeographies, the drawing order was standardized using the following sequence: ice sheets,  
mountains, landmasses and finally shallow marine environments (top to bottom layering).

150 Once the gaps are fixed, the consistency between the reconstructed paleogeography and paleobiology  
data can be tested. These tests are aimed at identifying inconsistencies between fossil-derived paleo-  
environments and underlying paleogeographies in order to improve the accuracy of marine-terrestrial  
boundaries in the paleogeographic maps. Fossil collections belonging to each time interval (Table 1)  
155 are first extracted from the dataset downloaded from the Paleobiology Database. Only the fossils with  
temporal ranges lying entirely within the corresponding time intervals were selected, as opposed to  
including the fossils that have larger temporal ranges. Fossils with temporal ranges crossing any time-  
interval boundary are not taken into consideration. As a result, a minimum number of fossil collections



160 were selected for each time interval. The selected fossil collections were classified into either terrestrial  
or marine setting category, according to a lookup table (Table 2). Alternatively, the terrestrial and  
marine fossil data could be separately downloaded from the Paleobiology Database. In this process,  
each fossil with a specific environment would be automatically oriented into the corresponding  
terrestrial or marine groups based on the same classification scheme (Table 2). Fossil collections would  
then be extracted in each time interval (Table 1) from terrestrial and marine fossils subgroups,  
165 respectively.

170 Fossil collections are then attached to the plate motion model of Matthews et al. (2016) so they can be  
reconstructed at each time interval. Subsequently, a point in polygon test is used to verify if the  
indicative paleo-environment (terrestrial or marine) of fossil collections is consistent with the  
underlying paleogeographic features. In this process, polygons are tested in the following sequence: ice  
sheets, mountains, landmasses and shallow marine environments. Terrestrial fossil paleo-environments  
correspond to landmass, mountain or ice sheet paleogeography. Fossil shallow marine environments  
175 map to marine environments in paleogeography.

Based on the inconsistencies between fossils paleo-environments and underlying paleogeographies, we  
can modify the terrestrial-marine boundaries in the paleo-maps. Figures 4 and 5 illustrate how to  
modify the marine-terrestrial boundaries in the paleogeographic maps based on the test results.  
180 Modifications are made according to the following rules: (1) Fossil collections from the Paleobiology  
Database are presumed to be well-dated, constrained geographically, not reworked and representative  
of their broader paleo-environments. Their indicative environments are assumed to be correct. (2) Only  
fossils within 100 km of the nearest terrestrial-marine boundary (for instance,  $d1 \leq 100$  km in Fig. 4b)  
are taken into account as valid proxies to improve marine-terrestrial boundaries. (3) The boundaries are  
185 shifted until the fossils environments are consistent with the underlying paleogeography and at the  
same time remain within about 20 km distance from the fossils used (Fig. 4c,  $d2 \approx 20$  km). (4) The  
adjacent boundary is accordingly adjusted and smoothed (Fig. 4c and Fig. 5c). (5) Occasionally, some  
adjacent fossils near the same boundary may indicate conflicting paleo-environments. In this case, we  
treat these adjacent fossils as a cluster, in which the environment represented by over 50% of fossils is  
190 considered to be indicative of the environment of the entire cluster. For example, the fossils in the  
black circle in Fig. 5b are regarded as a cluster, in which over 50% of fossils indicate a shallow marine  
environment. These rules are designed to maximize the use of paleobiology to improve paleogeography  
while attempting to minimize incorrect modifications. We note that in some cases the paleogeography  
cannot be fully reconciled with the Paleobiology Database (for example, inconsistent terrestrial fossils  
195 in the black circle in Fig. 5b).



200 However, in some rare cases, outlier fossils may be a deceptive recorder of paleogeography. For  
instance, Wichura et al. (2015) discussed the discovery of a beaked whale fossil 740 km inland from  
the present-day coastline of the Indian Ocean in the East Africa. The authors found evidence to suggest  
that this whale could have travelled inland from the Indian Ocean along an eastward-directed fluvial  
(terrestrial) drainage system and was stranded there, rather than representing a marine setting that  
205 would be implied under our assumptions. Therefore, theoretically, when using paleobiology to improve  
paleogeography, additional concerns about living habits of fossils and associated geological settings  
should be taken into account. In this study, we have removed this misleading fossil whale from the  
dataset. Such instances of deceptive fossils are rare.

## 210 4 Results

### 4.1 Paleobiology Tests

Global reconstructed paleogeographic maps from 402 to 2 Ma are tested against marine and terrestrial  
fossils that are reconstructed in the same rotation model (Matthews et al., 2016). The marine fossils  
215 consistency ratio is defined by the marine fossils within shallow marine paleogeographic polygons as a  
percentage of all marine fossils at the time interval, and in contrast, the marine fossils inconsistency  
ratio, by the marine fossils not within shallow marine paleogeography as a percentage of all marine  
fossils. Similarly, the terrestrial fossils consistency ratio is defined by the terrestrial fossils within  
landmass, mountain or ice sheet feature as a percentage of all terrestrial fossils at the time interval and  
220 the terrestrial fossils inconsistency ratio, by terrestrial fossils within shallow marine paleogeographic  
polygons as percentage of all terrestrial fossils at the time interval. Heine et al. (2015) applied a similar  
metric to evaluate global paleoshoreline models since the Cretaceous.

This test shows relatively high consistency between fossil paleo-environments and the underlying  
225 paleogeographic features (Fig. 6). The results since the Cretaceous are similar to that of Heine et al.  
(2015). In this study, the consistency ratios of marine and terrestrial fossils during 402-2 Ma both are  
generally over 50%, with an average of 74.8% (marine fossils, Fig. 6a, shaded area) and 77.1%  
(terrestrial fossils, Fig. 6b, shaded area) but both accompanying strong fluctuations over time. Only at  
the time interval of 402-380 Ma, the terrestrial fossils consistency ratio drops to approximately 20.0%,  
230 but this result is not reliable because there are only 18 terrestrial fossil collections available for this  
time interval.

235 The inconsistent marine and terrestrial fossils are used to improve marine-terrestrial boundaries in the  
paleogeographic maps according to the rules outlined in the Method section. Subsequently, the  
modified paleogeographies are tested using the same fossils. The results show the consistency ratios of  
marine and terrestrial fossils increased to average 97.1% (marine fossils, Fig. 6a, black line) and



240 average 85.9% (terrestrial fossils, Fig. 6b, black line) respectively after paleogeographies are modified  
and the overall fossils, rising from average 76.9% before modification (Fig. 6c, shaded areas) to  
average 96.1% after modification (Fig. 6c, black lines). Marine fossils (Fig. 6a, black lines) show better  
final consistency than terrestrial fossils (Fig. 6b, black lines), mainly because marine fossils records are  
less sparse than terrestrial fossils through time (Fig. 6d).

245 The sums of terrestrial and marine fossil collections change significantly over time (Fig. 6d), for  
example, more than 4200 in total within 269-248 Ma but less than 50 in 37-29 Ma. These variations  
could be due to the spatiotemporal sampling bias and incompleteness of the fossil record (Benton et al.,  
2000; Benson and Upchurch, 2013; Smith et al., 2012; Valentine et al., 2006), biota extinction and  
recovery (Hallam and Wignall, 1997; Hart, 1996) or our temporal selection criterion. In addition, the  
250 differences in the duration of geological time subdivisions lead to some time-intervals having shorter  
time spans that contain fewer fossil records. Specifically, marine fossils are generally more common  
than terrestrial fossils (Fig. 6d) as shallow marine environments can provide conditions that are more  
favorable to the preservation of biological organisms. As for the time intervals during which fossil data  
is scarce, paleobiology data is of limited use in improving paleogeography. For instance, there are less  
255 than 300 fossil collections in total in the time interval of 380-359 Ma mainly due to the late Devonian  
mass extinction (McGhee, 1996). However, additional records in the future will increase the usefulness  
of the Paleobiology Database in such instances.

#### 260 4.2 Improved Global Reconstructed Paleogeography

Based on the testing results of the time intervals, we can improve the marine-terrestrial boundaries in  
the global reconstructed paleogeographic maps using the approach described in Method section. The  
resulting improved global paleogeographic maps since the Devonian are presented in Figure 7.  
265 Although the modifications make the areal change minimally with regards to a global context, the  
resulting paleogeographies can provide us more accurate marine-terrestrial boundaries that would be  
important to generate precise paleoshorelines and therefore help constrain past changes in sea level and  
long-wavelength topography.

270 We subsequently calculate the area covered by each paleogeographic feature as a percentage of the  
Earth's total surface area at each time interval (Fig. 8b), using the HEALPix pixelization method that  
results in equal sampling of data on a sphere (Górski et al., 2005) and therefore equal sampling of  
surface areas. This method effectively excludes the effect of overlaps between paleogeographic  
geometries. Using the resulting percentages of the paleogeographic features at each time interval, we  
275 determine their surface areas on Earth (Fig. 8a) and their percentages accounting for the Earth's total  
surface area (Fig. 8b) for each time interval between 402 and 2 Ma.



280

As a result, the areas of landmass, mountain and ice sheet generally indicate increasing trends, while shallow marine and deep ocean areas show decreasing trends through time (Fig. 8). Overall, the computed areas are sequentially becoming larger in the order of ice sheet (average 1.0% of Earth surface), mountain (3.4%), shallow marine (14.2%), landmass (21.3%) and deep ocean (60.1%). Only in the time interval of 323-296 Ma, landmass and shallow marine areas are nearly equal at about 14.0%, and only during 359-285 Ma, ice sheet areas exceed mountain areas but ice sheets only exist during 380-285, 81-58, and 37-2 Ma. With Pangea formation in the latest Carboniferous or the Early Permian and breakup initiation in the Early Jurassic (Blakey, 2003; Domeier et al., 2012; Lenardic, 2016; Stampfli et al., 2013; Vai, 2003; Veever, 2004; Yeh and Shellnutt, 2016), these paleogeographic features areas change remarkably over time (Fig. 8). During 323-296 Ma (Late Carboniferous-the earliest Permian), landmasses reached their smallest area and subsequently underwent a rapid increase until they peaked at 26.7% in 224-203 Ma (Late Triassic). In contrast, ice sheets reached their largest area at that time. In the Early Jurassic of Pangea breakup, landmass areas rapidly decreased from 26.7% in 224-203 Ma to 24.6% in 203-179 Ma but shallow marine areas significantly increased by 3.7%.

285

290

295

#### 4.3 Global Continental Flooding History

300

We calculate the global flooding ratio of continental crust from 402 to 2 Ma (Fig. 9a, blue) by dividing the shallow marine area (Fig. 8a, lightblue) by the total continental area (inclusive of shallow marine, landmass, mountain and ice sheet; Fig. 9b, blue). The continental flooding ratios rapidly decrease from about 45.2% in the Late Devonian to 27.7% in 224-203 Ma of the Late Triassic, after that it peaks, with frequent fluctuations, at 41.8% in 94-81 Ma of the Late Cretaceous. That is then followed by a quick decrease again until it reaches the lowest point at 27.6% in 11-2 Ma.

305

### 5 Discussions

#### 5.1 Flooding history, global sea level changes, and assembly and breakup of Pangea

310

The continental flooding history we calculate between 402 and 2 Ma shows trends that are generally similar to global long-term sea level change (Haq et al., 1987; Haq et al., 2002; Müller et al., 2008; Fig. 9a). The eustatic sea level of Haq et al. (1987) and Haq et al. (2002) are inferred from the flooding ratios. Continental flooding decreases during Pangea amalgamation from the late Devonian until the Late Carboniferous, which is also reflected by low eustatic sea levels. Starting from the Early Jurassic with the breakup of Pangea, continental flooding is increased rapidly until the Late Cretaceous when it peaked at about 42.0%. This rapid increase could be explained by a reduction of ocean volume basin associated with a decrease of the average age of the ocean floor and an increase in mid-ocean ridge length during Pangea breakup (Hays and Pitman, 1973; Müller et al., 2008; Müller et al., 2016; Van

315



320 Avendonk et al., 2016). Since the Late Cretaceous, global continental flooding rapidly decreases again  
simultaneously with global sea level falling, which primarily reflects the increasing age of the ocean  
floor (Miller et al., 2005; Müller et al., 2008). Overall, the changes of the global continental flooding  
during 402-2 Ma are consistent with global long-term sea level changes.

### 325 **5.2 Emerged land areas, total continental areas, continental growth models, $^{87}\text{Sr}/^{86}\text{Sr}$ of ocean water, and assembly and breakup of Pangea**

330 We calculate the global emerged land areas since the Devonian from the improved global reconstructed  
paleogeographic features of landmass, mountain and ice sheet as percentages of the Earth's surface  
area (Fig. 9b, red). The results generally indicate ongoing increasing continental emergence varying  
from about 21.0% in the Devonian to nearly 30.0% in the Neogene. Emerged land areas were slightly  
larger between 58 and 2 Ma (up to 30%) and between 224 and 203 Ma (27.7%) than at present (27.5%).  
In contrast, the evolution of the emerged land areas is inverse to the global long-term sea level changes  
during this time (Fig. 9a), as expected.

335 Similarly, the total continental areas from 402 to 2 Ma are calculated from the improved global  
reconstructed paleogeographies including shallow marine, landmass, mountain and ice sheet. They  
show a sustained increase of continental areas, rising from 37.7% in 402-380 Ma to 41.1% in 11-2 Ma  
(Fig. 9b, green). Before the breakup of Pangea is initiated in the Late Triassic, the total continental  
areas generally remain constant at an average of about 38.0% of Earth's total surface area. Continental  
340 areas then increase between 203 and 179 Ma and peak at about 44.0% in the Early Neogene, followed  
by a sharp decrease ending up 41.1% in 11-2 Ma. The total continental areas from the latest Early  
Paleogene to the earliest Neogene were larger as compared to present-day continental area 42.5% of  
Earth's total surface area (Schubert and Reymers, 1985). Additionally, the differences between the total  
continental areas and emerged land areas over time indicate large submerged continental areas since  
345 the Late Paleozoic, which comprised an average of 14.0% of Earth's surface area.

A variety of continental growth models have been proposed (e.g. Armstrong, 1981; Veizer and Jansen,  
1979). Flament et al. (2013) present an integrated model to investigate the emerged area of continental  
crust as a function of continental growth. They predicted that the emerged land areas constantly  
350 increased from between ~21% and ~24% (CGM) at 402 Ma to 27% at 2 Ma, and the total continental  
area from between ~33% and ~38% (CGM) at 402 Ma to 42% at 2 Ma. Their results are generally  
consistent with the percentages of emerged land areas and total continental areas calculated in this  
study using paleogeographic features, despite some high frequency fluctuations in Early Jurassic and  
Late Cretaceous (Fig. 9b) indicated from our results.

355 The increase in the strontium isotope ratio ( $^{87}\text{Sr}/^{86}\text{Sr}$ ) recorded in marine carbonates was previously  
thought to reflect continental growth (e.g. Taylor and McLennan, 1985; Veizer and Jansen, 1979). The  
input of high radiogenic strontium from the continents to the oceans depends on the area of emerged



land and continental relief (Godderis and Veizer, 2000). Our calculated emerged land areas from  
360 Triassic to present show a similar changing trend with the evolution of  $^{87}\text{Sr}/^{86}\text{Sr}$  of ocean water  
(McArthur et al., 2012) although not for the older times (Fig. 9b). In contrast, the continental area in  
the entire timeframe appears not to indicate obvious consistency with the evolution of  $^{87}\text{Sr}/^{86}\text{Sr}$  of  
ocean water. Therefore, we confirm that  $^{87}\text{Sr}/^{86}\text{Sr}$  in ocean water may have good correlation with  
emerged land area (Godderis et al., 2014; van der Meer et al., 2017) rather than continental crust area  
365 (Flament et al., 2013).

## 6 Conclusions

Our study highlights the flexibility of digital paleogeographic models linked to state-of-the-art plate  
tectonic reconstructions in order to better understand the interplay of continental growth and eustasy,  
370 with wider implications for understanding Earth's paleotopography, ocean circulation, and the role of  
mantle convection in shaping long-wavelength topography. We present a workflow that enables the  
construction of paleogeographic maps with flexible spatial and temporal resolutions, while also  
becoming more testable and expandable with the incorporation of new paleo-environmental datasets.  
We also develop an approach to improve paleogeographic maps, especially the terrestrial-marine  
375 boundaries, using paleobiology data.

Comparing the continental flooding history since the late Devonian inferred from our improved global  
reconstructed paleogeographies with global long-term sea level change indicates that global continental  
flooding ratios are consistent with global sea level change. We calculate the global emerged land areas  
380 during 402-2 Ma from the improved global reconstructed paleogeographies. The evolution of the  
emerged land areas is inverse to global sea level changes during the time, as expected.

The total continental areas during 402-2 Ma, calculated from our improved reconstructed  
paleogeographies, shows good consistency with predictions of the long-term evolution of emerged land.  
385 The emerged land area from Triassic to present shows similar evolution with  $^{87}\text{Sr}/^{86}\text{Sr}$  record of ocean  
water, while the total continental crust area does not. This confirms that the change of  $^{87}\text{Sr}/^{86}\text{Sr}$  in  
ocean water through time reflects fluctuations in emerged land area rather than in continental crust area.

## Supplementary data

We provide the shapefiles of the global paleogeographic maps during 402-2 Ma improved using  
390 paleobiology, the GeoTiff files of all these maps, the paleobiology data in shapefile used in this study,  
an animation for the improved global paleogeographic maps, and a README file outlined the  
workflow of this study. All supplementary material can be downloaded from the link  
(<https://www.dropbox.com/sh/jzsrnnpgrdzpaa/AAAShE5xhDxrIhmKpoBaa1G4a?dl=0>).

## Acknowledgements



395 This work was supported by Australian Research Council grants ARC grants IH130200012 (RDM, SZ), DE160101020 (NF) and SIEF RP 04-174 (SW). We thank Julia Sheehan and Logan Yeo for digitizing these paleogeographic maps, and John Cannon and Michael Chin for help with GPlates and pyGPlates.

### References

- 400 Amante, C., Eakins, B. and Boulder, C.: ETOPO1 1 arc-minute global relief model: Procedures, data sources and analysis, NOAA Technical Memorandum, 2009.
- Armstrong, R. L.: Radiogenic isotopes: the case for crustal recycling on a near-steady-state no-continental-growth Earth, *Philos. Trans. R. Soc. Lond. Ser. A* 301, 443–471, 1981.
- Benson, R. B. J. and Upchurch, P.: Diversity trends in the establishment of terrestrial vertebrate eco-  
 405 systems: interactions between spatial and temporal sampling biases, *Geology*, 41, 43–46, 2013.
- Benton, M. J., Wills, M. A., and Hitchin, R.: Quality of the fossil record through time, *Nature*, 403, 534–537, 2000.
- Blakey, R.: Carboniferous Permian global paleogeography of the assembly of Pangaea. In: Symposium on Global Correlations and Their Implications for the Assembly of Pangea, Utrecht (August 10-  
 410 16, 2003), International Congress on Carboniferous and Permian Stratigraphy, p. 57. International Commission on Stratigraphy, 2003.
- Domeier, M.: A plate tectonic scenario for the Iapetus and Rheic oceans. *Gondwana Res.*, 36, 275–295, 2016.
- Domeier, M., Van der Voo, R., and Torsvik, T. H.: Paleomagnetism and Pangea: the road to  
 415 reconciliation, *Tectonophysics*, 514–517, pp. 14–43, 2012.
- Flament, N., Coltice, N., and Rey, P. F.: The evolution of the  $^{87}\text{Sr}/^{86}\text{Sr}$  of marine carbonates does not constrain continental growth, *Precambrian Research*, 229, 177–188, 2013.
- Goddéris, Y., Donnadieu, Y., Le, Hir. G., and Lefebvre, V.: The role of palaeogeography in the Phanerozoic history of atmospheric  $\text{CO}_2$  and climate, *Earth-Science Reviews*, 128, 122–138, 2014.
- 420 Godderis, Y. and Veizer, J.: Tectonic control of chemical and isotopic composition of ancient oceans: the impact of continental growth, *Am. J. Sci.*, 300, 434–461, 2000.
- Golonka, J.: Late Triassic and Early Jurassic palaeogeography of the world, *Palaeogeography, Palaeoclimatology, Palaeoecology*, 244, 297–307, 2007.
- Golonka, J., Krobicki, M., Pajak, J., Giang, N. V., and Zuchiewicz, W.: Global Plate Tectonics and  
 425 Palaeogeography of Southeast Asia, Faculty of Geology, Geophysics and Environmental Protection, AGH University of Science and Technology, Arkadia, Krakow, Poland, 2006.
- Golonka, J., Ross, M.I., and Scotese, C.R.: Phanerozoic paleogeographic and paleoclimatic modeling maps, in: Embry, A.F., Beauchamp, B., Glass, D.J. (Eds.), *Pangea: Global Environment and Resources*, Memoir-Canadian Society of Petroleum Geologists, vol. 17, pp. 1–47, 1994.
- 430 Górski, K. M., Hivon, E., Banday, A. J., Wandelt, B. D., Hansen, F. K., Reinecke, M., and Bartelmann, M.: HEALPix: A Framework for High-Resolution Discretization and Fast Analysis of Data Distributed on the Sphere, *The Astrophysical Journal*, 622: 759–771, 2005.



- Gurnis, M., Müller R. D., and Moresi, L.: Dynamics of Cretaceous to the present vertical motion of Australia and the Origin of the Australian- Antarctic Discordance, *Science*, 279, 1499–1504, 1998.
- 435 Hallam, A. and Wignall, P.B.: Mass extinctions and their aftermath. Oxford: Oxford University Press, 320p, 1997.
- Haq, B. U., Hardenbol, J., and Vail, P. R.: Chronology of fluctuating sea levels since the Triassic, *Science*, 235, 1156–1167, 1987.
- Haq, B. U. and Schutter, S. R.: A chronology of Paleozoic sea-level changes. *Science*, 322, 64–68,
- 440 2008.
- Hart, M. B.: Biotic recovery from mass extinction events. Geological Society of London Special Publication 102, 1996.
- Hays, J. D. and Pitman, W. C.: Lithospheric plate motion, sea level changes and climatic and ecological consequences, *Nature*, 246, 18–22, 1973.
- 445 Heine, C., Yeo, L. G., and Müller, R. D.: Evaluating global paleoshoreline models for the Cretaceous and Cenozoic. *Aust. J. Earth Sci.*, 62, 275–287, 2015.
- Lenardic, A.: Plate tectonics: A supercontinental boost, *Nature Geoscience*, doi:10.1038/ngeo2862, 2016.
- Matthews, K. J., Maloney, K. T., Zahirovic, S., Williams, S. E., Seton, M. and Müller, R. D.: Global plate boundary evolution and kinematics since the late Paleozoic. *Global and Planetary Change*, 146, 226–250, 2016.
- 450 McArthur, J. M., Howarth, R. J., and Shields, G. A.: Strontium isotope stratigraphy. In: Gradstein, F. M., Ogg, J. G., Schmotz, M. D., Ogg, G. M. (Eds.), *The Geological Time Scale 2012*. Elsevier, pp. 127–144, 2012.
- 455 McGhee, G. R.: *The Late Devonian Mass Extinction: the Frasnian/Famennian crisis*. New York: Columbia University Press, 1996.
- Miller, K. G., Kominz, M. A., Browning, J. V., Wright, J. D., Mountain, G. S., Katz, M. E., Sugarman, P. J., Cramer, B. S., Christie-Blick, N., and Pekar, S. F.: The Phanerozoic record of global sea-level change, *Science*, 310:1293–1298, 2005.
- 460 Müller, R. D., Sdrolias, M., Gaina, C., Steinberger, B., and Heine, C.: Long-term sea-level fluctuations driven by ocean basin dynamics, *Science*, 319, 1357–1362, 2008.
- Müller, R. D., Seton, M., Zahirovic, S., Williams, S. E., Matthews, K. J., Wright, N. M., Shephard, G. E., Maloney, K. T., Barnett-Moore, N., Hosseinpour, M., Dan, J. B., and John, C.: Ocean basin evolution and global-scale reorganization events since Pangea breakup, *Annual Review of Earth and Planetary Science Letters*, 44, 107-138, 2016.
- 465 Ronov, A., Khain, V., and Balukhovskiy, A.: *Atlas of Lithological-Paleogeographical Maps of the World, Mesozoic and Cenozoic of Continents and Oceans*, U.S.S.R. Academy of Sciences, Leningrad, 79 pp, 1989.
- Ronov, A., Khain, V., and Sestlavinsky, K.: *Atlas of Lithological-Paleogeographical Maps of the World, Late Precambrian and Paleozoic of Continents*, U.S.S.R. Academy of Sciences, Leningrad, 70 pp,
- 470 1984.



- Salles, T., Flament, N., and Müller, D.: Influence of mantle flow on the drainage of eastern Australia since the Jurassic Period, *Geochem. Geophys. Geosyst.*, 18, doi:10.1002/2016GC006617, 2017.
- 475 Schubert, G. and Reymer, A. P. S.: Continental volume and freeboard through geological time, *Nature*, 316 (6026), 336–339, 1985.
- Scotese, C.: A continental drift flipbook, *The Journal of Geology*, 112, 729–741, doi: 10.1086/424867, 2004.
- Sloss, L.: Tectonic evolution of the craton in Phanerozoic time, *The Geology of North America*, 2, 25–51, 1988.
- 480 Smith, A. B., Lloyd, G. T., and McGowan, A. J.: Phanerozoic marine diversity: rock record modelling provides an independent test of large-scale trends, *Proceedings of the Royal Society B: Biological Sciences* 279, 4489–4495, 2012.
- Smith, A. G., Smith, D. G., and Funnell, B. M.: *Atlas of Mesozoic and Cenozoic Coastlines*, Cambridge University Press, Cambridge, 99 pp, 1994.
- 485 Spasojevic, S. and Gurnis, M.: Sea level and vertical motion of continents from dynamic Earth models since the Late Cretaceous, *American Association of Petroleum Geologists Bulletin*, 96, 2037–2064, doi:10.1306/03261211121, 2012.
- Stampfli, G. M., Hochard, C., Vérard, C., Wilhem, C. and vonRaumer, J.: The formation of Pangea. *Tectonophysics*, 593, 1–19, 2013.
- 490 Taylor, S. R., McLennan, S. M.: *The Continental Crust: Its Composition and Evolution*, Blackwell Scientific Publications, 328 p, 1985.
- Vai, G. B.: Development of the palaeogeography of Pangaea from Late Carboniferous to Early Permian, *Paleogeography, Palaeoclimatology, Palaeoecology*, 196, 125–155, 2003.
- Valentine, J. W., Jablonski, D., Kidwell, S., and Roy, K.: Assessing the fidelity of the fossil record by using marine bivalves, *Proceedings of the National Academy of Sciences*, 103, 6599–6604, 2006.
- 495 Van Avendonk, H. J. A., Davis, J. K., Harding, J. L., and Lawver, L. A.: Decrease in oceanic crustal thickness since the breakup of Pangaea, 10, doi: 10.1038/NGEO2849, 2016.
- van der Meer, D. G., van den Berg van Saparoea, A. P. H., van Hinsbergen, D. J. J., van de Weg, R. M. B., Godderis, Y., Le Hir, G., and Donnadieu, Y.: Reconstructing first-order changes in sea level during the Phanerozoic and Neoproterozoic using strontium isotopes, *Gondwana Research*, 44, 22–34, 2017.
- 500 Veevers, J. J.: Gondwanaland from 650–500 Ma assembly through 320 Ma merger in Pangea to 185–100 Ma breakup: supercontinental tectonics via stratigraphy and radiometric dating, *Earth-Science Reviews*, 68, 1–132, 2004.
- 505 Veizer, J. and Jansen, S. L.: Basement and sedimentary recycling and continental evolution, *J. Geol.*, 87, 341–370, 1979.
- Wichura, H., Jacobs, L. L., Lin, A., Polcyn, M. J., Manthi, F. K., Winkler, D. A., Strecker, M. R., and Clemens, M.: A 17-My-old whale constrains onset of uplift and climate change in east Africa, *Proc. Natl. Acad. Sci. U.S.A.*, 112(13), 3910–3915, 2015.



510 Wright, N., Zahirovic, S., Müller, R. D., and Seton, M.: Towards community-driven paleogeographic  
reconstructions: integrating open-access paleogeographic and paleobiology data with plate  
tectonics, *Biogeosciences*, 10, 1529–1541, doi:10.5194/bg-10-1529-2013, 2013.

Yeh, M. W. and Shellnutt, J. G.: The initial break-up of Pangaea elicited by Late Palaeozoic  
deglaciation, *Scientific Reports*, 6: 31442, doi: 10.1038/srep31442, 2016.

515

520

525

530

535

540

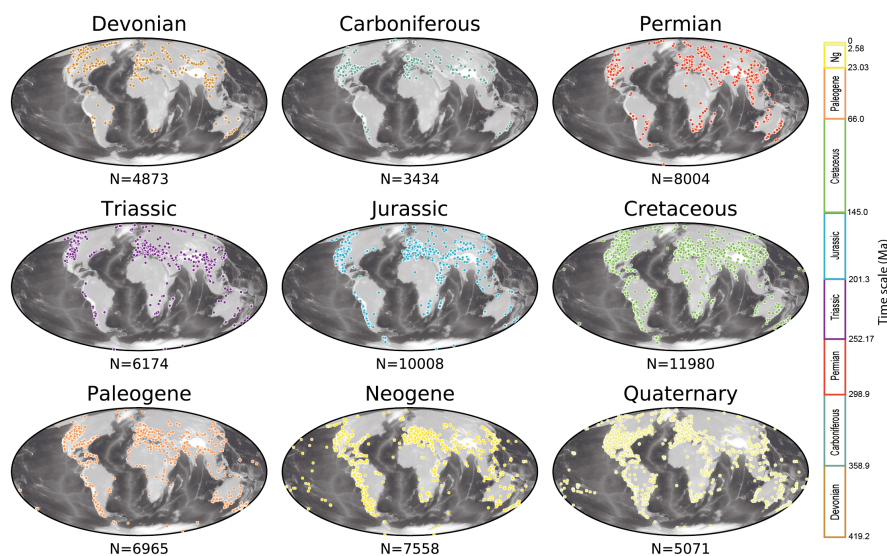
545



550

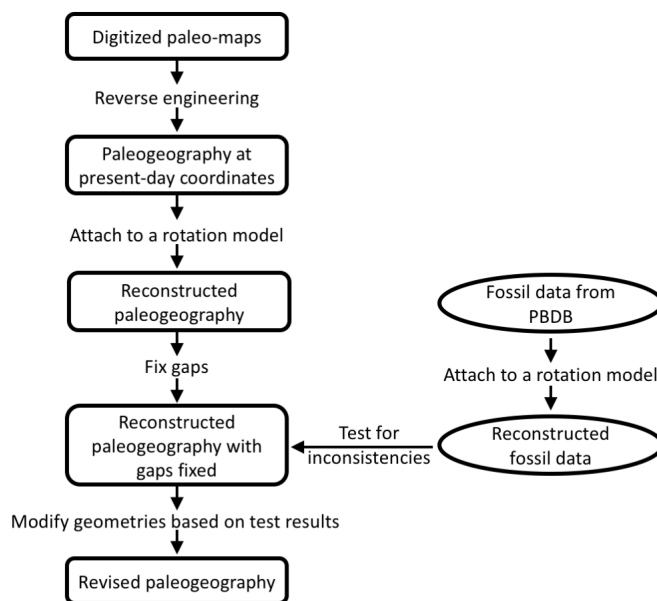
**Table 1.** Time scale of Golonka et al. (2006)'s paleo-maps since the Early Devonian, their numerical equivalents as defined by Sloss (1998), and corresponding reconstruction times.

Era	Epoch	Nominal Age	Sloss (1988)		Reconstruction
			Start Age (Ma)	End Age (Ma)	Time (Ma)
Cenozoic	Tortonian-Gelasian	Late Tejas III	11	2	6
	Burdigalian-Serravallian	Late Tejas II	20	11	14
	Chattian-Aquitainian	Late Tejas I	29	20	22
	Priabonian Rupelian	Early Tejas III	37	29	33
	Lutetian-Bartonian	Early Tejas II	49	37	45
	Thanetian-Ypresian	Early Tejas I	58	49	53
Mesozoic	Late Cretaceous-earliest Paleogene	Late Zuni IV	81	58	76
	Late Cretaceous	Late Zuni III	94	81	90
	Early Cretaceous-earliest Late Cretaceous	Late Zuni II	117	94	105
	Early Cretaceous	Late Zuni I	135	117	126
	latest Late Jurassic-earliest Early Cretaceous	Early Zuni III	146	135	140
	Middle Jurassic-Late Jurassic	Early Zuni II	166	146	152
	Middle Jurassic	Early Zuni I	179	166	169
	Early Jurassic-earliest Middle Jurassic	Late Absaroka III	203	179	195
	Late Triassic-earliest Jurassic	Late Absaroka II	224	203	218
	Early-earliest Late Triassic	Late Absaroka I	248	224	232
Paleozoic	Late Permian	Early Absaroka IV	269	248	255
	Early Permian	Early Absaroka III	285	269	277
	latest Carboniferous-earliest Permian	Early Absaroka II	296	285	287
	Late Carboniferous	Early Absaroka I	323	296	302
	Early Carboniferous	Kaskaskia IV	338	323	328
	latest Devonian-Early Carboniferous	Kaskaskia III	359	338	348
	Middle-Late Devonian	Kaskaskia II	380	359	368
	Early-Middle Devonian	Kaskaskia I	402	380	396



555

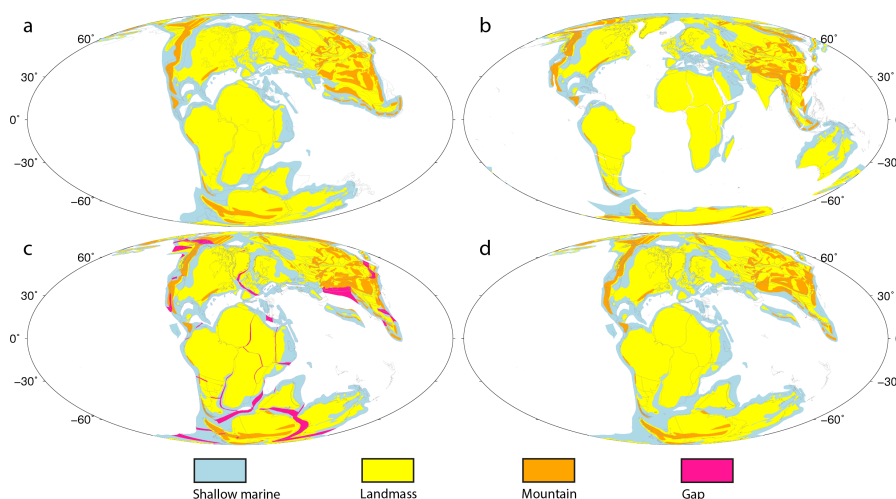
**Fig. 1.** Global distributions and numbers of fossil collections since the Devonian. The greyscale background shows global present-day topography ETOPO1 (Amante and Eakins, 2009) with lighter shades corresponding to increasing elevation. Fossil collections from the Paleobiology Database are colored according following the standard used by the International Commission on Stratigraphy.



560

Fig. 2. Workflow used to reverse-engineer paleogeographic reconstructions and revise them using paleobiology data. PBDB: Paleobiology Database.

565



570

Fig. 3. (a) Reconstructed paleogeography from Golonka et al. (2006) at 126 Ma. (b) Global paleogeography at 126 Ma in present-day coordinates. (c) Global paleogeography at 126 Ma reconstructed using the plate motion model of Matthews et al. (2016). Gaps are highlighted in pink. (d) Global paleogeography at 126 Ma reconstructed using the reconstruction of Matthews et al. (2016) with gaps fixed by filling with adjacent paleo-environment attributes. Gray lines indicate reconstructed present-day coastlines and terrane boundaries. Mollweide projection with 0°E central meridian.

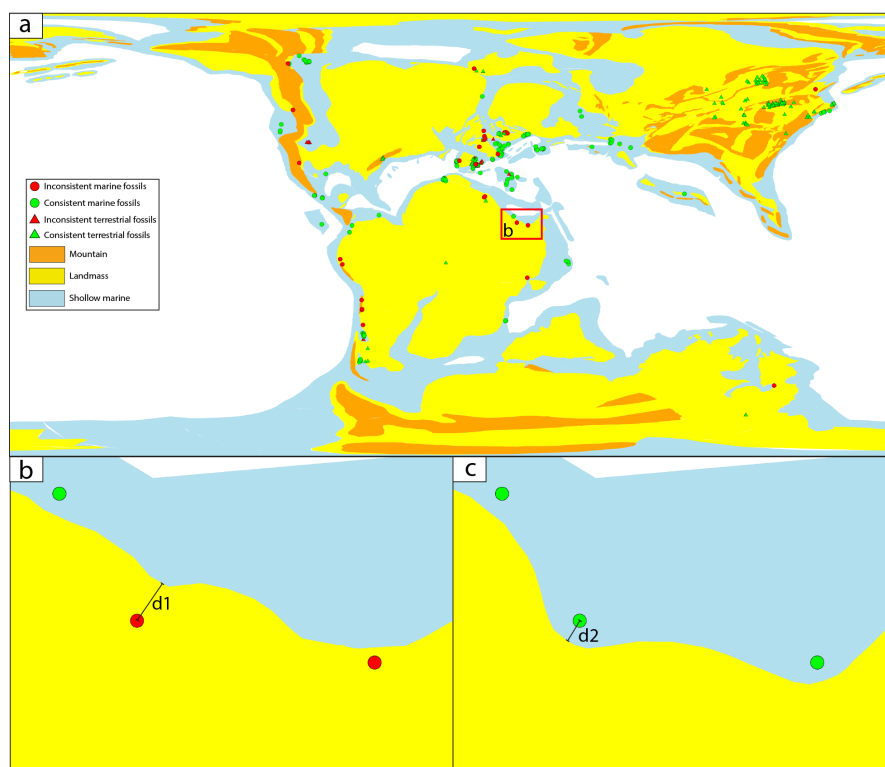


575

**Table 2. A lookup table for classifying fossils indicating different paleo-environments into marine or terrestrial settings and their corresponding paleogeographic types presented in Golonka et al. (2006). Terrestrial fossil paleo-environments correspond to paleogeographic features of landmasses, mountains or ice sheets, and marine fossil paleo-environments to shallow marine environments.**

Marine		Terrestrial	
Paleogeography	Fossil Paleoenvironments	Paleogeography	Fossil Paleoenvironments
Shallow marine environments	marine indet.	basinal (carbonate)	terrestrial indet.
	carbonate indet.	basinal (siliceous)	fluvial indet.
	peritidal	marginal marine indet.	alluvial fan
	shallow subtidal indet.	coastal indet.	channel lag
	open shallow subtidal	estuary/bay	coarse channel fill
	lagoonal/restricted shallow subtidal	lagoonal	fine channel fill
	sand shoal	paralic indet.	channel
	reef, buildup or bioherm	delta plain	wet floodplain
	perireef or subreef	interdistributary bay	dry floodplain
	intrashelf/intraplatform reef	delta front	floodplain
	platform/shelf-margin reef	prodelta	crevasse splay
	slope/ramp reef	deltaic indet.	levee
	basin reef	foreshore	mire/swamp
	deep subtidal ramp	shoreface	fluvial-lacustrine indet.
	deep subtidal shelf	transition zone/lower shoreface	delta plain
	deep subtidal indet.	offshore	fluvial-deltaic indet.
	offshore ramp	submarine fan	lacustrine - large
offshore shelf	basinal (siliciclastic)	lacustrine - small	
offshore indet.	deep-water indet.		
slope		Ice sheets	glacial
		Landmasses/Mountains	pond
			crater lake
			lacustrine delta plain
			lacustrine interdistributary bay
			lacustrine prodelta
			lacustrine deltaic indet.
			lacustrine indet.
			dune
			interdune
			loess
			eolian indet.
			cave
			fissure fill
			sinkhole
			karst indet.
			tar
			spring

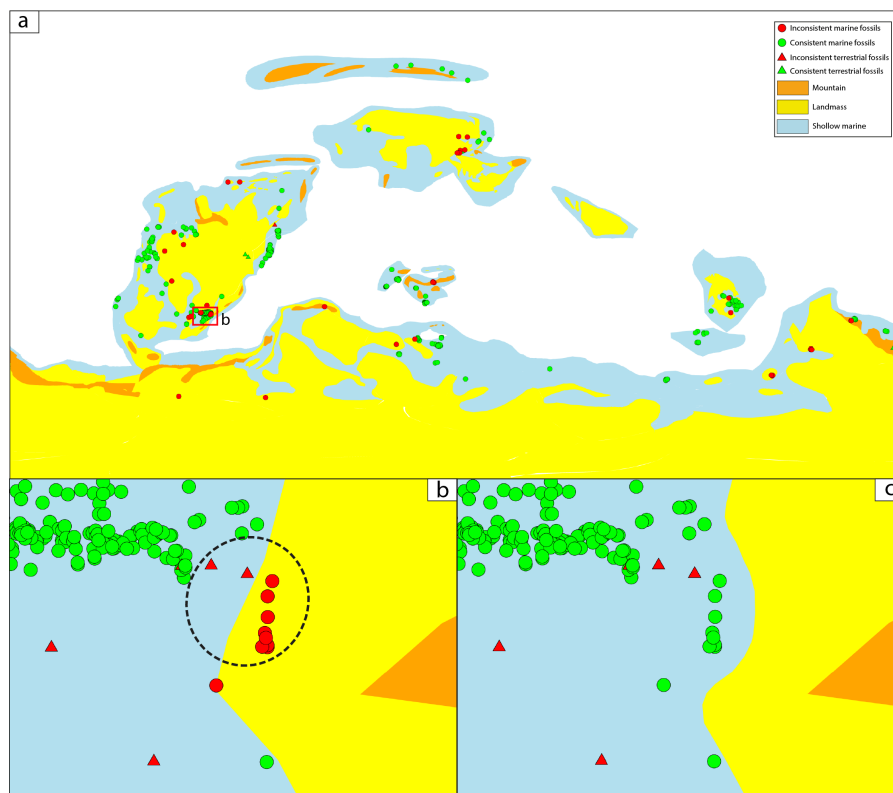
580



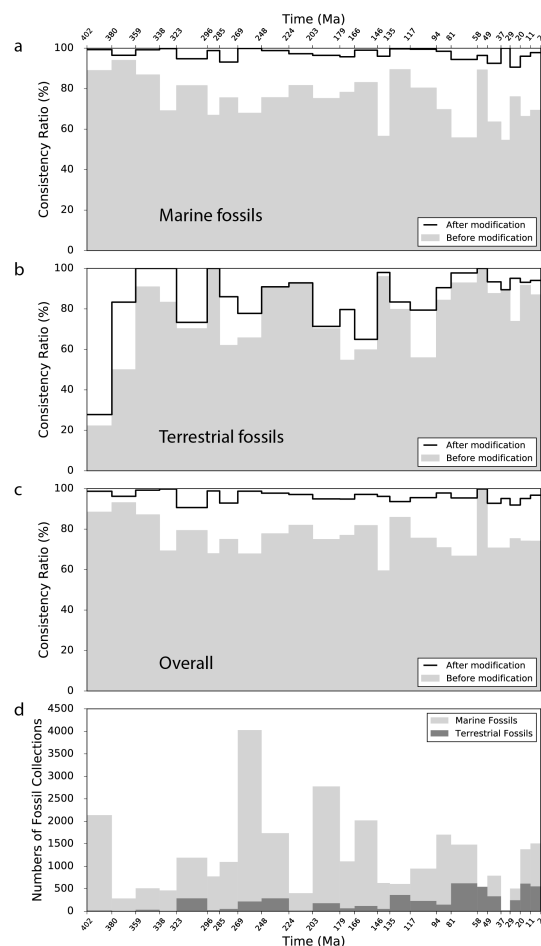
585

**Fig. 4.** (a) Global paleogeography at 126 Ma (Golonka et al., 2006) reconstructed using the model of Matthews et al. (2016) tested against terrestrial and marine fossil collections recorded in the Paleobiology Database. (b) The zoomed-in area of the small box in (a) highlights inconsistent marine fossils (red points).  $d1 \leq 100$  km is the distance between the inconsistent marine fossil and its nearest terrestrial-marine boundary. (c) illustrates how a terrestrial-marine boundary is modified based on inconsistent fossils, the terrestrial-marine boundary is shifted until the two marine fossils are consistent with the underlying paleogeography and at the same time keep about 20 km distance from their nearest boundary,  $d2 \approx 20$  km is the distance between the fossil used and its nearest terrestrial-marine boundary shifted.

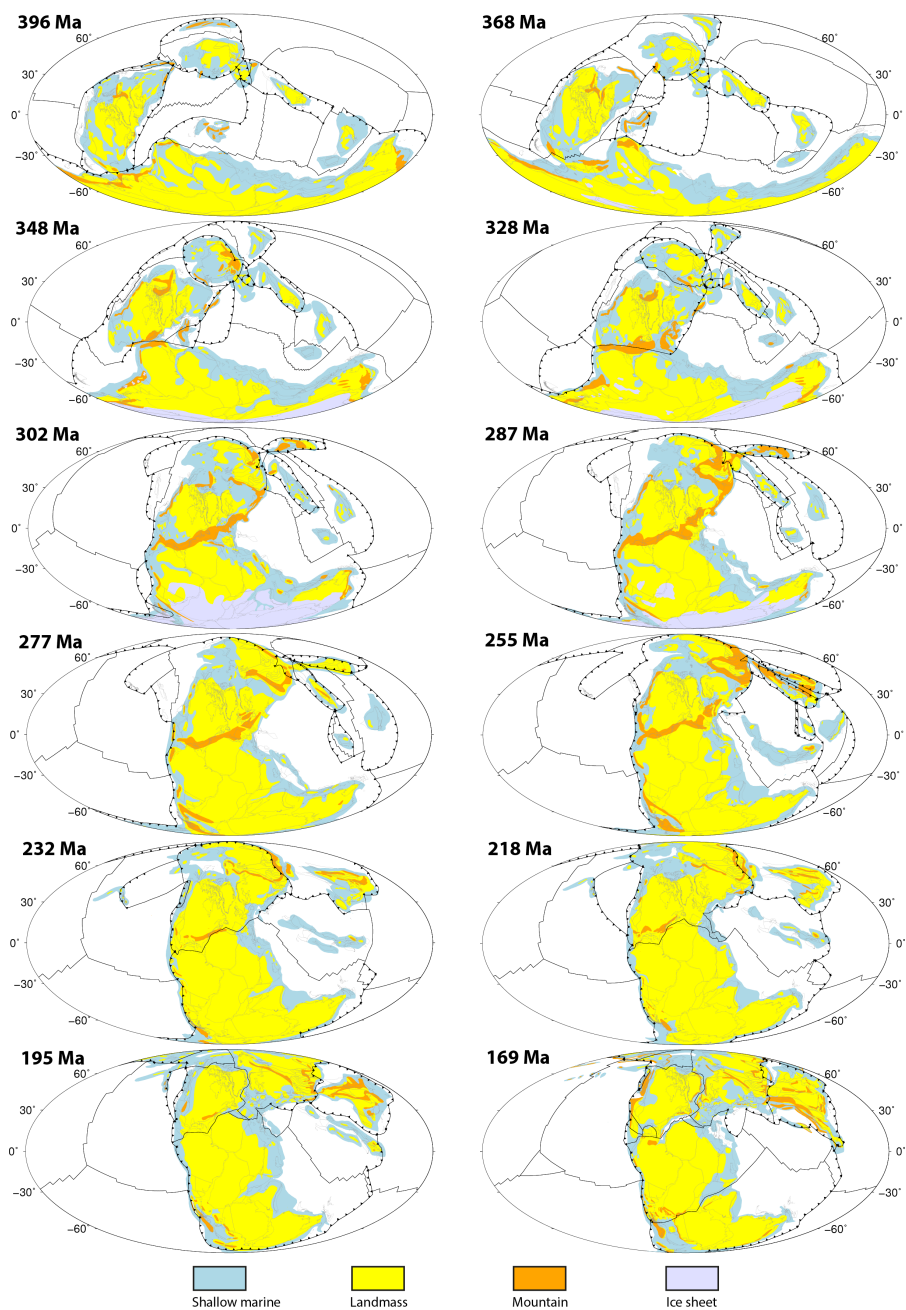
595



600 Fig. 5. (a) Global paleogeography reconstructed at 396 Ma tested by terrestrial and marine fossils. (b) Zoomed-in area of the small box in (a). The fossils in the black circle are considered as a cluster, in which over 50% of fossils indicate shallow marine environment, therefore, the whole cluster is interpreted as shallow marine. (c) Illustrates how the terrestrial-marine boundary is shifted to be reconciled with fossil collections.



605 Fig. 6. (a) Global consistency ratios between marine fossils and underlying paleogeographies before (shaded  
 areas) and after (black lines) modification based on fossils for each time interval between 402 and 2 Ma. (b)  
 610 Global consistency ratios between terrestrial fossils and underlying paleogeographies before (shaded areas)  
 and after (black lines) modification for each time interval between 402 and 2 Ma. (c) Global consistency  
 ratios between total fossils (marine and terrestrial) and underlying paleogeographies before (shaded areas)  
 and after (black lines) modification for each time interval between 402 and 2 Ma. (d) Numbers of terrestrial  
 (shaded in dark grey) and marine (shaded in light grey) fossil collections for each time interval between 402  
 and 2 Ma.



615

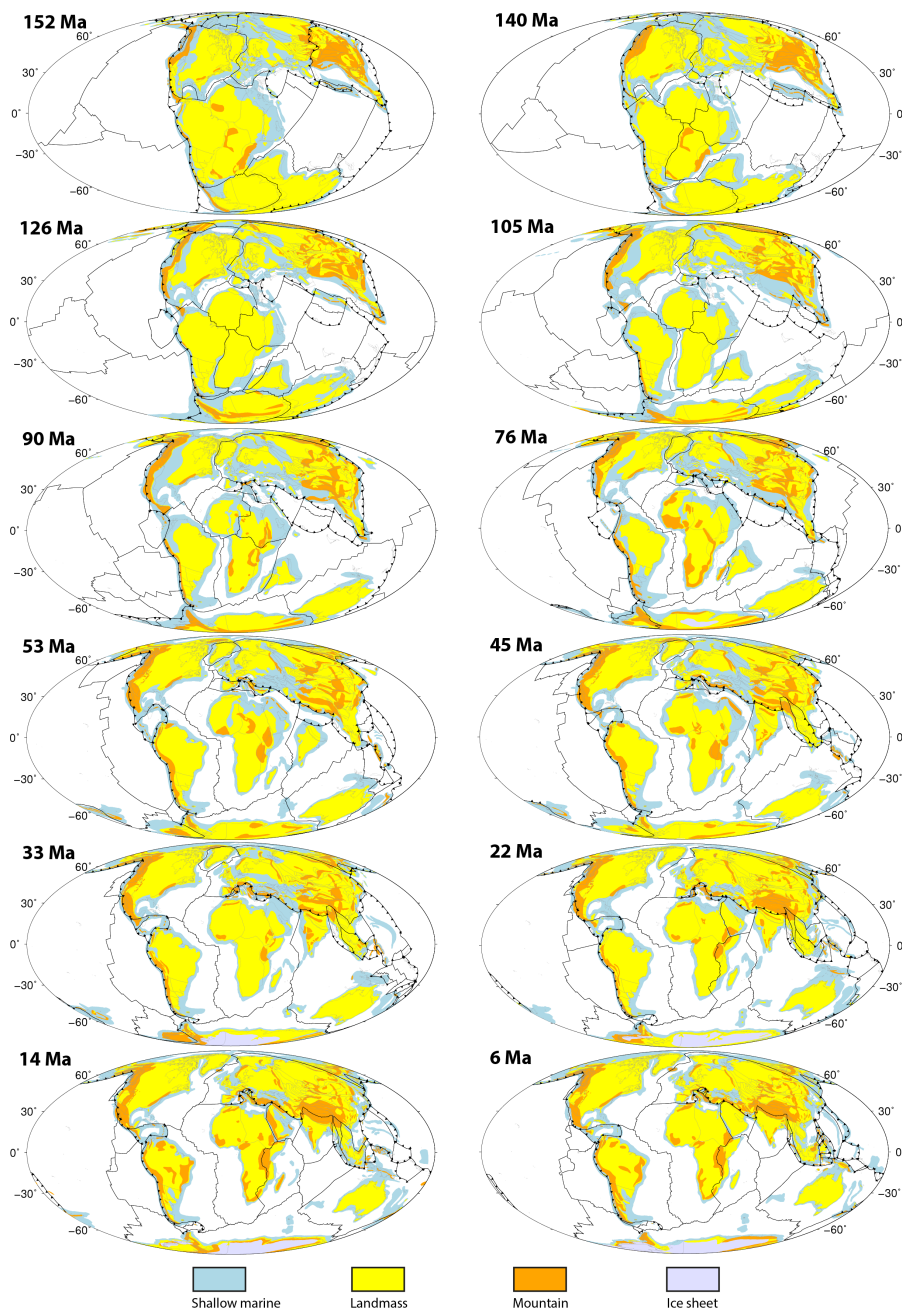
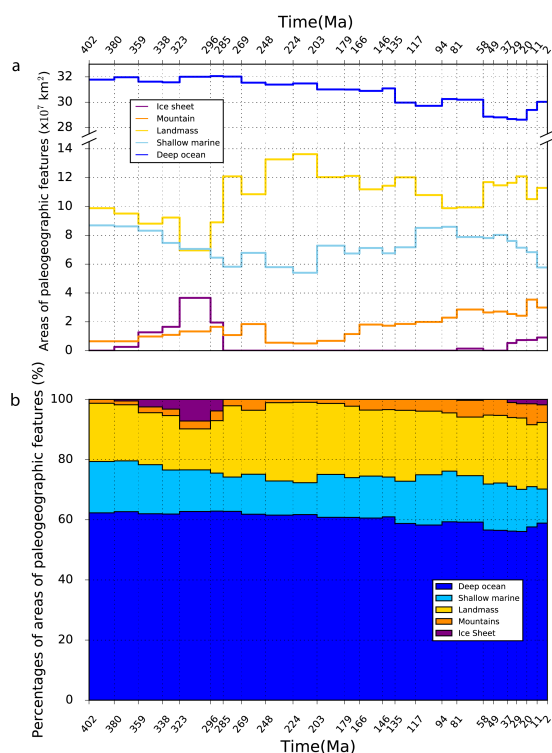


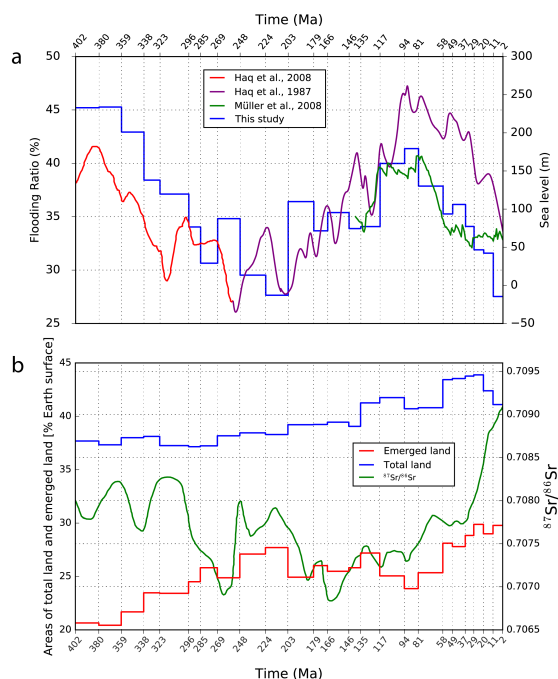
**Fig. 7.** Global paleogeographies from 402 to 2 Ma reconstructed with the plate reconstruction of Matthews et al. (2016) and improved using paleobiology data. Black toothed lines indicate subduction zones, and other black lines denote mid-ocean ridges and transforms. Gray outlines delineate reconstructed present-day coastlines and terranes. Mollweide projection with 0°E central meridian.

620



625

Fig. 8. (a) Global paleogeographic feature surface areas from 402 to 2 Ma. (b) Global paleogeographic feature areas as percentages of the Earth's total surface area at each time interval from 402 to 2 Ma.



630 **Fig. 9. (a) Global continental flooding ratio since the Devonian (blue) and global sea level from Haq et al. (1987) (purple), Haq et al. (2008) (red) and Müller et al. (2008) (green). (b) Total continental areas (blue) and emerged land areas (red) as a percentage of Earth's surface area.  $^{87}\text{Sr}/^{86}\text{Sr}$  record of ocean water of McArthur et al. (2012) (Green). Total continental area comprises shallow marine, landmass, mountain and ice sheet. Emerged land comprises landmass, mountain and ice sheet. Flooding ratio is defined as shallow**  
 635 **marine area divided by the total continental area.**

635